Mathematical Modeling and Validation of the Aerial Robot Control System with the Pixhawk Flight Controller

Amin Rajawana and Pruittikorn Smithmaitrie
Department of Mechanical Engineering, Prince of Songkla University, Hat Yai, Songkhla, Thailand
Email: amin.rajawana@gmail.com, pruittikorn.s@psu.ac.th

***Abstract*—Modeling of an aerial robotic control system for cooperative working robots initially needs a mathematical model of the robot. This work presents a validated cross configuration quadcopter model with the stabilized flight control system. Coefficients and parameters regarding the stability control of the aerial robot, i.e., throttle-to-RPM conversion, thrust coefficient, torque coefficient and moment of inertia, are obtained by the experiments. These measured parameters yield the better flight simulation compared with the product datasheet values. Then, the experimental coefficients and parameters are defined in the MATLAB/Simulink model based on Newton-Euler equations. This study analyzes system responses and simulates the flight stability controlled system of the Pixhawk flight controller in the horizontal plane and vertical direction. After that, the flight response of the mathematical model is compared with the actual flight response. The results show that the model of the UAV flight control system has similar characteristic to the actual flight. Thus, the presented mathematical model and control parameters could be adopted for further design on the aerial robot control system such as a multi-robot cooperative task.**

***Index Terms*—quadcopter, mathematical model, PID controller, pixhawk, flight controller, experimental validation**

I. Introduction

Recently, the unmanned aerial vehicle (UAV), commonly known as drone [1], has been adopted to various works and activities. Common examples of UAV applications are search and rescue (SAR) [2,3], infrastructure maintenance [4], agricultural management [5], supporting law enforcement [6], aerial photography [7,8], forest monitoring [9], 3D mapping [10], traffic management [11] and cooperative transportation [12,13]. For the cooperative work of UAVs in transportation, many techniques or knowledge are implemented to the system integration, for instance, cooperative control of swarm UAVs [14–16], leader-and-follower formation [17–20], precise localization of terrestrial objects [21], feedback controller design [22], as well as modeling and simulation of the cooperative UAV system [22–24]. However, the new knowledge and technique must be validated before implementation on the UAV in order to minimize the risk due to the crash of system failure. One of the best practice is to simulate by a validated mathematical model.

Mathematical modeling of multiple aerial robots for object transportation is rather complicated comparing with a single UAV modeling. However, validation of the UAV model must be done first. Then, the validated UAV model is duplicated and mathematically connected to be developed for the multi-UAV cooperative system. Thus, this work aims to validate the UAV model as the beginning step before the further study of the multiple aerial robot cooperative system. The crucial issue which influences model accuracy is the primary input parameters of the aerial robot. Many parameters can be taken from the specification datasheet but the best way is to acquire by measuring and testing.

This study presents the validate mathematical model, input parameters and three experimental setups to obtain them. First, the motor coefficients are obtained by testing the motor behavior which required a force/torque sensor. Second, the UAV moment of inertia is measured by the bifilar torsional pendulum testing which related to the natural frequency. Third, the model of flight stability control system is validated by comparing the simulated flight response with the actual flight response. All details are presented in the following sections.

II. Methodoly and Experimental Setup

The aerial robot platform is a X-copter frame of 640 mm in diagonal length (L). The Pixhawk flight controller is selected to be developed as the mathematical flight controller model. It has a 32-bit processor unit with an additional failsafe backup controller extensive memory. It is easy to set up and directly work with many ground control station softwares such as Mission Planner. The ground control station (GCS) provides the autonomous flight features and UAV's flight paths [25]. The four T-Motor Antigravity 4006 KV380 brushless DC motors drive the four Tarot 1555 foldable propellers that installed on each of the motor. The electronic speed controllers (ESC), Hobbywing XRotor 40A, control speed of the motors. The UAV system is supplied by a 6S 5400 mAh Lithium polymer battery.

Manuscript received December 2, 2019; revised June 15, 2020.

doi: 10.18178/ijmerr.9.7.1065-1071

These components are integrated as the tested UAV platform to determine their parameters for the mathematical model development. They are motor coefficient, moment of inertia and stabilization control parameters as follows.

A. Motor Testing

The Experimental setup to determine the motor characteristics is shown in Fig.1. A microcontroller (Arduino Mega 1280) generates PWM signal feeding to the ESC, starting from 0 to 100% PWM by increasing 5% every 5 seconds. An IR sensor detects propeller rotation and sends the signal to the microcontroller to calculate the rotational speed of the rotor. The force/torque sensor (ATI Industrial Automation, Model Gamma), installed under the motor base, senses the produced force and torque. All of the sensing information are recorded in a computer and calculated the percent of throttle conversion to the rotational speed, thrust coefficient and torque coefficient. The component connection diagram is shown in Fig.2.

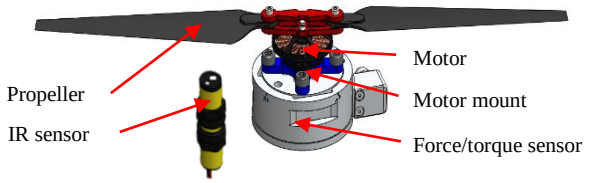

Figure 1. The experimental setup to determine the motor characteristics.

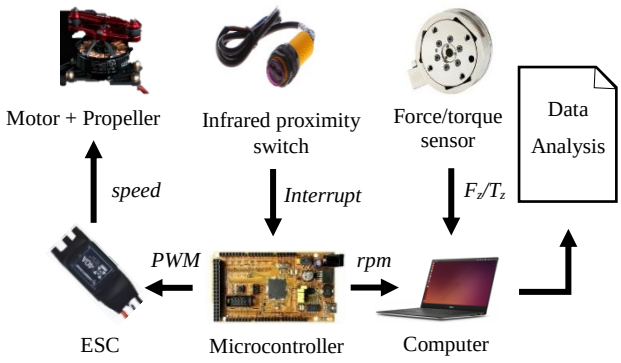

Figure 2. The component connection diagram of the motor testing.

The percent throttle conversion coefficient (C_{R}) is determined by the relationship of the percent throttle command and motor rotational speed. It can be written as

$$\omega = C_{R1}(\%\,\text{throttle})^2 + C_{R2}(\%\,\text{throttle}) + C_{R3} \quad (1)$$

where ω is the steady-state motor rotational speed [rpm], % throttle is the percentage of the throttle command, C_{R1}, C_{R2} and C_{R3} are the % throttle to RPM conversion coefficients.

The coefficient of thrust (C_{T}) provides a conversion from the rotor speed to the thrust that lifts the UAV. It can be written as

$$T = c_{\mathrm{T}}\rho A_{\mathrm{r}} r^2 \omega^2 \quad (2)$$

where T is the thrust [N], c_{T} is the thrust coefficient of the rotor, ρ is the density of air [kg/m^3], A_{r} is the cross-sectional area of the propeller's rotation [m^2] and r is the radius of the rotor [m]. For a simple flight model, it can be simplified by merging the constant parameters as [26]

$$T = C_{\mathrm{T}}\omega^2 \quad (3)$$

To understand effect of the motor on the UAV rotation about the yaw axis, the motor torque and propeller speed relationship must be determined, similar to the thrust. The torque coefficient (C_{Q}) converses the motor rotational speed to the generated torque (Q) as [26]

$$Q = C_{\mathrm{Q}}\omega^2 \quad (4)$$

B. Moment of Inertia

Mass moment of inertia is an important parameter to develop an accurate UAV dynamic model. For simple structures, mass moment of inertia can be obtained by a CAD software or mathematical analysis. For complex structures which include many subcomponents, the moment of inertia must be measured. The bifilar vertical-axis torsional pendulum is a simple and cost-effective method to determine the mass moment of inertia of rigid bodies as shown in Fig. 3. The UAV is suspended by two parallel vertical wires that free to rotate about its attached points. The restoring torque of the bifilar pendulum relates to the gravitational force. The body rotation causes the tested object to rise slightly [27].

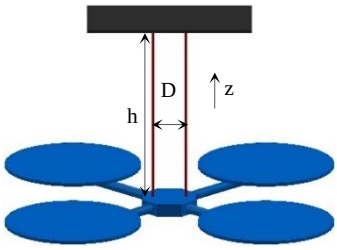

Figure 3. The bifilar torsional pendulum setup.

Then, the hanging quadrotor is rotated about the axis of interest (z-axis) with a small angle (θ), and it rises up for the height of z. The weight of the UAV provides the restoring torque which generates the rotational response of the system. The moment of inertia about the axis of interest is obtained from the natural frequency of the oscillation. The relationship between the moment of inertia and natural frequency is [28]

$$I = \frac{mgD^2}{4h\omega_n^2} \quad (5)$$

where I is the moment of inertia about the rotational axis [kg.m^2], m is the mass of the tested object [kg], g is the gravitational acceleration constant [m/s^2], D is the distance between the two suspended wires [m], h is the length of the wire [m] and ω_n is the natural frequency [rad/s].

C. Modeling and Simulation

The simulation package used in this study is adopted from Quad-Sim [29]. This package supports MATLAB/Simulink for dynamic modeling and simulation of quadcopter control system. In this study, the parameters of the controller model are developed to comply with the Pixhawk flight controller by replacing the original PI-P controller with the P-PID controller and P-P-PID controller for stabilizing the UAV in horizontal plane and vertical direction, respectively. The proposed system block diagram is consistent with the Pixhawk control scheme as shown in Fig. 4 [30]. The scale factor of each axis is for adjusting output range of the simulation response to match with the experimental response.

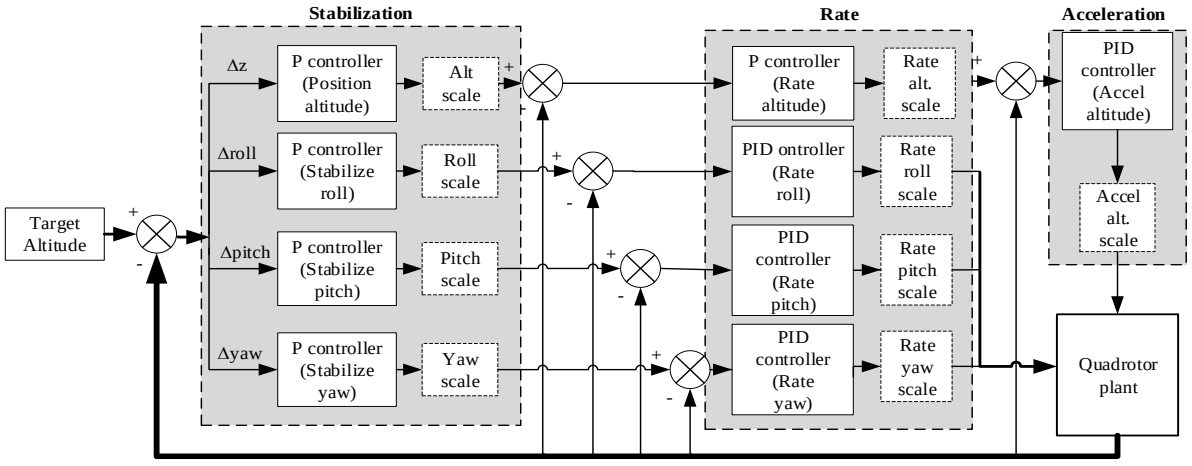

Figure 4. The system block diagram of the Pixhawk flight controller.

A standard procedure to determine system parameters is usually defined in terms of the system step response. As shown in Fig.5, the overshoot is the amount of system output that exceeds the desired steady-state response where P.O. is the percentage of overshoot. The rise time (t_r) is the time of a system that takes for the response to rise from 10% to 90% of the step input magnitude. The settling time (t_s) is the time required for the system output to settle within 2% of the input amplitude. The steady-state error (e_{ss}) is the difference between actual and desired input values for a long period that the transient response has decayed and left only the continuous response [31].

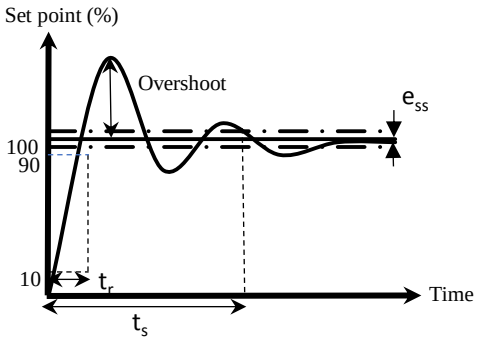

Figure 5. System response and characteristics to the step input.

Accordingly, the coefficient C_R, C_T, and C_Q from the motor testing and the moment of initial I_{xx}, I_{yy}, and I_{zz} are substituted into the mathematical model. The actual PID control gains from the Pixhawk controller are also transferred to the model. Then, the controller outputs of the model are adjusted by the scaling factors to make the simulation flight response match the real flight response.

III. Result and Discussion

A. The Percent Throttle Conversion Coefficient

When the percent throttle increases, the motor speed increases as written in the quadratic equation (1). The conversion coefficient can be estimated by the quadratic fitting curve according to the testing results as shown in Fig. 6. The motor starts rotating at the 15% throttle with the motor speed of 720 rpm. For every 5% throttle increment until 100% throttle, the motor rotational speed is recorded. The maximum motor speed at 100% throttle is about 6,000 rpm. Accordingly, the calculated conversion coefficients are C_{R1} = -0.467, C_{R2} = 116.0 and C_{R3} = -1,064. The coefficient of determination (R^2) is 99.04 %, which confirm the quadratic relationship.

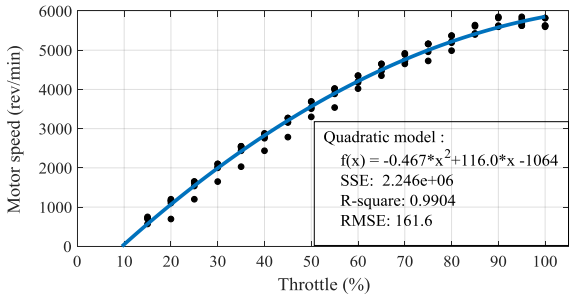

Figure 6. The relationship between the throttle percentage and motor rotational speed.

B. The Thrust Coefficient

By knowing the relationship between the % throttle and motor speed, it is possible to vary motor speed by changing the % throttle according to (1). The thrust increases linearly to the square of the motor speed as written in (3). The conversion of the motor speed to the propeller thrust, called the thrust coefficient, is calculated by the linear regression of the experimental result as shown in Fig.7. In this case, the thrust coefficient (C_T) is $6.035x10^{-7}$ N/rpm^2. The determination is 99.54 %. The maximum thrust is about 20 N.

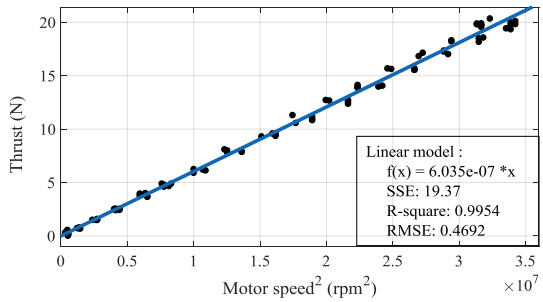

Figure 7. The relationship between the thrust and square of motor rotational speed.

C. The Torque Coefficient

The relationship between the % throttle and motor speed yields the measurement of the torque response when the motor speed changes regarding the throttle percentage as written in (1) and (4). The torque coefficient can be calculated by linear regression based on the experimental data as shown in Fig. 8. The torque coefficient is 1.230×10^{-8} N.m/rpm^2. The coefficient of determination is 99.44 %. The maximum torque is about 0.4 N.m.

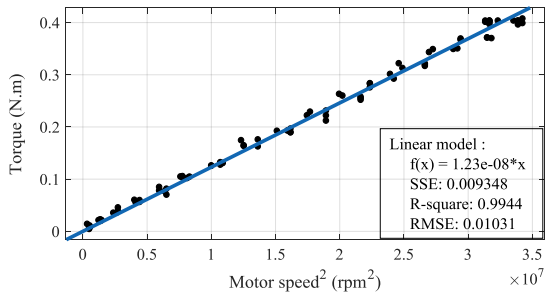

Figure 8. The relationship between the torque and square of motor rotational speed.

D. The Moment of Inertia of the UAV

Based on the bifilar pendulum experimental setup, the quadcopter is rotated for 45° and released to oscillate freely for 1 minute. When the estimated initial angles are around 18°, 4° and 2° of the roll, pitch and yaw axes, respectively, the vibration amplitude is recorded by the IMU sensor in the Pixhawk controller. The sample rate is 50 Hz. The rotational tests are done on the roll, pitch and yaw axes, separately. The initial offset of the measured data is removed by using the detrending method which removes a trend from a time series; the trend usually refers to a change in the mean value over time. The results are shown in Fig.9.

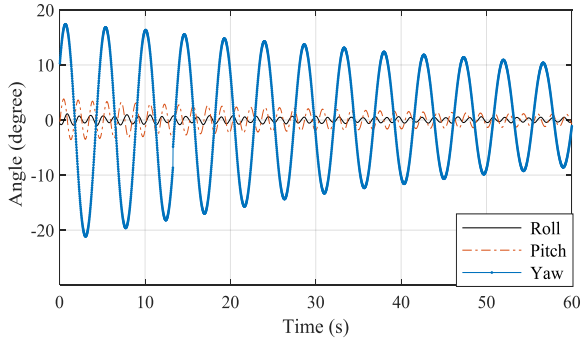

Figure 9. The bifilar pendulum test of the UAV.

Then, the vibration responses of the UAV in Fig.9 are converted from the time domain to the frequency domain by using the fast Fourier transform (FFT) algorithm. The major frequencies of the rotation about each axis are below 1 Hz as shown in Fig.10.

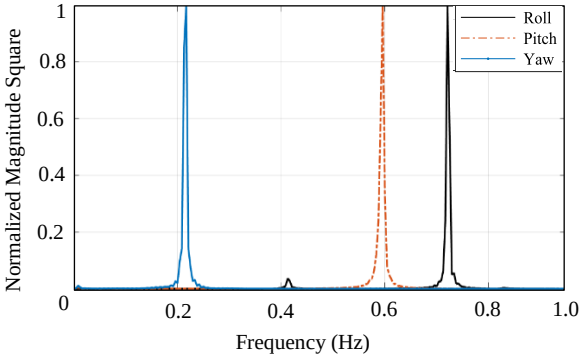

Figure 10. The oscillation of the UAV bifilar test in the frequency domain.

The experimental setup parameters (D and h) in Fig.3 are different for each of the rotational axis as shown in Table I. Consequently, the major natural frequencies and calculated moment of inertia of all axes are determined.

TABLE I. THE TESTING PARAMETERS, NATURAL FREQUENCIES AND MOMENT OF INERTIA OF THE UAV.

Axis	D (m)	h (m)	f_n (Hz)	I (kg.m^2)
Roll	0.110	0.330	0.7208	0.0115
Pitch	0.180	0.390	0.5958	0.0381
Yaw	0.0850	0.420	0.2125	0.0621

E. Validation of the UAV Mathematical Model

All parameters from the motor and inertia testing are summarized in Table II . These parameters are defined in the MATLAB/Simulink model. The actual Pixhawk controller gains of the quadcopter are tuned by the auto-tune algorithm. Then, the stability and trajectory control gains of the UAV are used in the mathematical model as shown in Table III. The stabilized, rate, and accelerated scaling factors of each model controller are only tuned in order to make the flight response of the mathematical model close to the actual flight response.

TABLE II. PARAMETERS OF THE UAV MODEL.

Variable	Values	
I_{xx}	0.0115	kg.m^2
I_{yy}	0.0381	kg.m^2
I_{zz}	0.0621	kg.m^2
m	2.6232	kg
L	0.640	m
C_{R1}	-0.467	rpm
C_{R2}	116.0	rpm
C_{R3}	-1,064	rpm
C_T	6.035×10^{-7}	N/rpm^2
C_Q	1.23×10^{-8}	N.m/rpm^2

TABLE III. THE CONTROL GAINS AND SCALES FOR THE STABILITY CONTROL SYSTEM MODEL.

	Axis		Stabilization		Rate		Acceleration	
			Gain	Scale	Gain	Scale	Gain	Scale
Stability Control loop	Roll	P	4.5	1.0	0.135	9.0	-	-
		I	-		0.09		-	
		D	-		0.0036		-	
	Pitch	P	4.5	3.0	0.135	8.0	-	-
		I	-		0.09		-	
		D	-		0.0036		-	
	Yaw	P	4.5	0.3	0.18	60	-	-
		I	-		0.018		-	
		D	-		0		-	
Trajectory Control loop	Altitude	P	1.0	0.35	5	2.7	0.5	1.0
		I	-		-		1.0	
		D	-		-		0	

In the actual flight test and simulation, the UAV is ordered to take off and hold its position at 10 m above the ground. The UAV flight response is recorded. The IMU signals provide the UAV rotation about the roll, pitch and yaw axes. The barometer indicates the UAV altitude. On the other hand, the UAV model with the Pixhawk controller is also simulated with the same flight plan. The actual flight and simulation results are plotted as shown in Figs. 11-14.

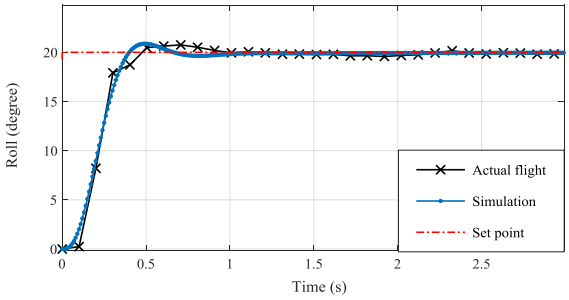

Figure 11. The UAV flight response to the step roll input.

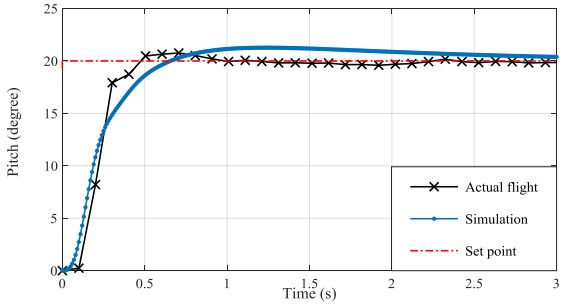

Figure 12. The UAV flight response to the step pitch input.

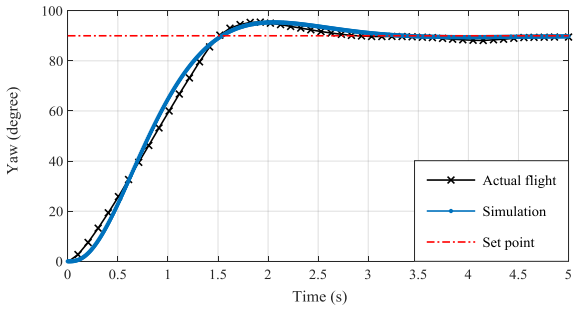

Figure 13. The UAV flight response to the step yaw input.

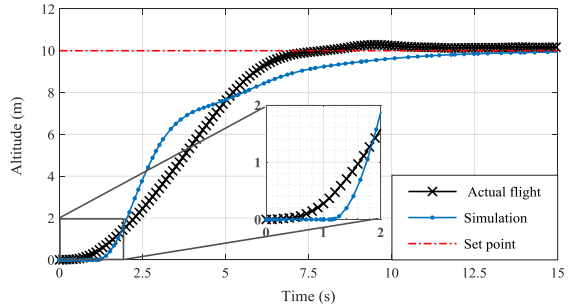

Figure 14. The UAV flight response to the step altitude input.

The plot comparison (Figs. 11-14) shows that the flight simulation has similar responses to the actual flight, especially on the roll and yaw axes. In Fig. 14, the first 2 seconds response of the actual altitude is quicker than the simulation response. This may due to the vortex changes in near-ground which increases the initial air velocity at the air inlet section on the top of the rotor, resulting in the additional thrust [32]. This phenomenon is also known as the aerodynamic ground effect as illustrated in Fig. 15.

The system characteristics of the simulation and actual UAV are summarized in Table IV. Based on Figs. 11-14 and Table IV, it is found that the UAV model gives the stabilized and altitude flight responses closed to the actual flight, in terms of P.O., t_r, t_s, and e_{ss}. However, there are some differences between the actual and simulation flight responses in terms of t_r and t_s. That may cause by time response of the barometer, wind effect, and ground effect which are not included in the simulation.

TABLE IV. THE UAV AND SIMULATION FLIGHT CHARACTERISTICS.

Response	Flight	System Characteristic			
		P.O.	t_r	t_s	e_{ss}
Roll	Actual flight	3.79	0.30	1.01	0.15
	Simulation	3.01	0.28	0.63	0.06
	Error	0.78	0.02	0.38	0.09
Pitch	Actual flight	5.27	0.20	1.31	0.09
	Simulation	6.36	0.34	1.89	0.56
	Error	-1.09	-0.14	-0.58	-0.47
Yaw	Actual flight	6.04	1.11	2.73	0.74
	Simulation	5.34	0.97	2.79	0.45
	Error	0.70	0.14	-0.06	0.29
Altitude	Actual flight	0.00	4.24	7.05	0.19
	Simulation	0.00	4.12	8.31	0.14
	Error	0.00	0.12	-1.26	0.05

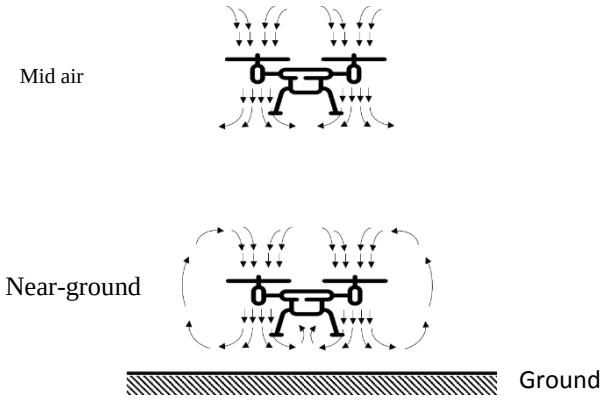

Figure 15. The aerodynamic ground effect.

IV. CONCLUSION

In this work, the UAV system parameters such as the percent throttle to motor speed, force and torque coefficients, moment of inertia of a quadcopter have been experimentally determined. The UAV model with the Pixhawk flight controller is developed in MATLAB/Simulink. The control algorithm of the UAV model emulates the Pixhawk controller. The simulated controller gains are from the actual flight auto-tuned gains. The scaling factor is added into the simulated controller model in order to adjust the simulation flight response to match with the actual flight response. This is because there are other physical effects need to be compensated in the simulation such as the change of atmospheric wind speed and pressure, aerodynamic ground effect and response time of the sensors which are not initially included in the simulation model. The results have shown that the model flight characteristic is similar to the actual flight. Thus, the presented mathematical model and control parameters could be adopted for further design on the aerial robot control system such as a multi-robot cooperative task.

CONFLICT OF INTEREST

The authors declare no conflict of interest.

AUTHOR CONTRIBUTIONS

P.S. conceived and designed the research investigation; P.S. contributed analysis tools; A.R. performed the experiment and collected the data; A.R. and P.S. analyzed the data and wrote the paper; Both authors had approved the final version.

ACKNOWLEDGMENT

This research is supported by the National Research Council of Thailand (Grant No. NRCT162/2561). The support is gratefully acknowledged. Pruittikorn Smithmaitrie is the corresponding author (Email: pruittikorn.s@psu.ac.th).

REFERENCES

[1] M. Hassanalian and A. Abdelkefi, "Classifications, applications, and design challenges of drones: A review," *Prog. Aerosp. Sci.*, vol. 91, pp. 99–131, May 2017.
[2] A. B ̈ackman *et al.*, "Drones for provision of flotation support in simulated drowning," *Air Med. J.*, vol. 37, no. 3, pp. 170–173, May 2018.
[3] A. Claesson *et al.*, "Drones may be used to save lives in out of hospital cardiac arrest due to drowning," *Resuscitation*, vol. 114, pp. 152–156, May 2017.
[4] T. Rakha and A. Gorodetsky, "Review of Unmanned Aerial System (UAS) applications in the built environment: Towards automated building inspection procedures using drones," *Autom. Constr.*, vol. 93, pp. 252–264, Sep. 2018.
[5] B. S. Faiçal *et al.*, "The use of unmanned aerial vehicles and wireless sensor networks for spraying pesticides," *J. Syst. Archit.*, vol. 60, no. 4, pp. 393–404, Apr. 2014.
[6] J. Straub, "Unmanned aerial systems: Consideration of the use of force for law enforcement applications," *Technol. Soc.*, vol. 39, pp. 100–109, Nov. 2014.
[7] H. Zhao *et al.*, "Aerial photography flight quality assessment with GPS/INS and DEM data," *ISPRS J. Photogramm. Remote Sens.*, vol. 135, pp. 60–73, Jan. 2018.
[8] H. Liu, M. Lin, and L. Deng, "UAV route planning for aerial photography under interval uncertainties," *Optik*, vol. 127, no. 20, pp. 9695–9700, Oct. 2016.
[9] J. Zhang, J. Hu, J. Lian, Z. Fan, X. Ouyang, and W. Ye, "Seeing the forest from drones: Testing the potential of lightweight drones as a tool for long-term forest monitoring," *Biol. Conserv.*, vol. 198, pp. 60–69, Jun. 2016.
[10] P. Urbanová, M. Jurda, T. Vojtíšek, and J. Krajsa, "Using drone-mounted cameras for on-site body documentation: 3D mapping and active survey," *Forensic Sci. Int.*, vol. 281, pp. 52–62, Dec. 2017.
[11] T. Jiang, J. Geller, D. Ni, and J. Collura, "Unmanned aircraft system traffic management: Concept of operation and system architecture," *Int. J. Transp. Sci. Technol.*, vol. 5, no. 3, pp. 123–135, Oct. 2016.
[12] G. Loianno and V. Kumar, "Cooperative transportation using small quadrotors using monocular vision and inertial sensing," *IEEE Robot. Autom. Lett.*, vol. 3, no. 2, pp. 680–687, Apr. 2018.
[13] E. N. Barmpounakis, E. I. Vlahogianni, and J. C. Golias, "Unmanned aerial aircraft systems for transportation engineering: Current practice and future challenges," *Int. J. Transp. Sci. Technol.*, vol. 5, no. 3, pp. 111–122, Oct. 2016.
[14] E. de Vries and K. Subbarao, "Cooperative control of swarms of unmanned aerial vehicles," in *49th AIAA Aerospace Sciences Meeting including the New Horizons Forum and Aerospace Exposition*, Orlando, Florida, 2011, pp.1-23.

[15] J. Hu and A. Lanzon, "An innovative tri-rotor drone and associated distributed aerial drone swarm control," *Robot. Auton. Syst.*, vol. 103, pp. 162–174, May 2018.
[16] R. R. McCune and G. R. Madey, "Swarm control of UAVs for cooperative hunting with DDDAS," *Procedia Comput. Sci.*, vol. 18, pp. 2537–2544, Jan. 2013.
[17] Z. Lin, W. Ding, G. Yan, C. Yu, and A. Giua, "Leader–follower formation via complex Laplacian," *Automatica*, vol. 49, no. 6, pp. 1900–1906, Jun. 2013.
[18] M. B. Vankadari, K. Das, and S. Kumar, "Autonomous leader-follower architecture of A.R. drones in GPS constrained environments," in *Proceedings of the Advances in Robotics on - AIR '17*, New Delhi, India, 2017, pp. 1–6.
[19] Z. Hou and I. Fantoni, "Distributed leader-follower formation control for multiple quadrotors with weighted topology," in *2015 10th System of Systems Engineering Conference (SoSE)*, 2015, pp. 256–261.
[20] F. Wu, J. Chen, and Y. Liang, "Leader-follower formation control for quadrotors," *IOP Conf. Ser. Mater. Sci. Eng.*, vol. 187, p. 012016, Mar. 2017.
[21] F. Betti Sorbelli, S. K. Das, C. M. Pinotti, and S. Silvestri, "Range based algorithms for precise localization of terrestrial objects using a drone," *Pervasive Mob. Comput.*, vol. 48, pp. 20–42, Aug. 2018.
[22] G. Wu and K. Sreenath, "Geometric control of multiple quadrotors transporting a rigid-body load," in *53rd IEEE Conference on Decision and Control*, 2014, pp. 6141–6148.
[23] I. H. B. Pizetta, A. S. Brandão, and M. Sarcinelli-Filho, "Cooperative quadrotors carrying a suspended load," in *2016 International Conference on Unmanned Aircraft Systems (ICUAS)*, 2016, pp. 1049–1055.
[24] A. S. Aghdam, M. B. Menhaj, F. Barazandeh, and F. Abdollahi, "Cooperative load transport with movable load center of mass using multiple quadrotor UAVs," in *2016 4th International Conference on Control, Instrumentation, and Automation (ICCIA)*, 2016, pp. 23–27.
[25] "Pixhawk Overview — Copter documentation." [Online]. Available: http://ardupilot.org/copter/docs/common-pixhawk-overview.html. [Accessed: 10-Apr-2019].
[26] R. Mahony, V. Kumar, and P. Corke, "Multirotor aerial vehicles: modeling, estimation, and control of quadrotor," *IEEE Robot. Autom. Mag.*, vol. 19, no. 3, pp. 20–32, Sep. 2012.
[27] M. R. Jardin and E. R. Mueller, "Optimized measurements of unmanned-air-vehicle mass moment of inertia with a bifilar pendulum," *J. Aircr.*, vol. 46, no. 3, pp. 763–775, May 2009.
[28] M. L. Ireland, "Investigations in multi-resolution modelling of the quadrotor micro air vehicle," Ph.D. thesis, University of Glasgow, 2014, pp. 51-52.
[29] "Quad-Sim - File Exchange - MATLAB Central." [Online]. Available: https://www.mathworks.com/matlabcentral/fileexchange/48053. [Accessed: 10-Apr-2019].
[30] "Altitude Hold Mode — Copter documentation." [Online]. Available: http://ardupilot.org/copter/docs/altholdmode.html. [Accessed: 10-Apr-2019].
[31] R. C. Dorf and R. H. Bishop, *Modern Control Systems*, 12th ed. Prentice Hall: Pearson, 2010.
[32] B. J. Emran and H. Najjaran, "A review of quadrotor: An underactuated mechanical system," *Annual Reviews in Control*, vol. 46, pp. 165-180, Oct. 2018.

Amin Rajawana received his B.Eng. degree in Mechatronics Engineering from Prince of Songkla University, Thailand, in 2016. Currently, he is a student of Master in Mechanical Engineering from Prince of Songkla University. His research interests robotics, unmanned aerial vehicles and image processing.

Pruittikorn Smithmaitrie received his B.Eng. degree in mechanical engineering from Prince of Songkla University, Thailand, in 1996. After his graduation, he had received the Royal Thai Government Scholarship to pursue his M.S. and Ph.D. degrees in the United States. in 2000, he obtained the M.S. degree in mechanical engineering from Vanderbilt University, Nashville, TN. in 2004, he received the Ph.D. degree in mechanical engineering from University of Kentucky, Lexington, KY. He has been a faculty member of the Mechanical Engineering Department, Prince of Songkla University, since 1996 and became an Associate Professor in 2008. His research interests are the analysis and design of mechatronic systems, robotics and piezoelectric applications.